arXiv:2412.20933v1 [q-bio.BM] 30 Dec 2024

ProtScan: Modeling and Prediction of RNA-Protein Interactions

Gianluca Corrado[1], Michael Uhl[2], Rolf Backofen[2,3], Andrea Passerini[1], and Fabrizio Costa[*2,4]

[1] ***Department of Information Engineering and Computer Science, University of Trento, Trento, 38123, Italy***

[2] ***Department of Computer Science, University of Freiburg, Freiburg, 79110, Germany***

[3] ***BIOSS Centre for Biological Signalling Studies, Cluster of Excellence, University of Freiburg, Freiburg, 79110, Germany***

[4] ***Department of Computer Science, University of Exeter, Exeter EX4 4QF, UK***

Abstract

Motivation: CLIP-seq methods are valuable techniques to experimentally determine transcriptome-wide binding sites of RNA-binding proteins. Despite the constant improvement of such techniques (e.g. eCLIP), the results are affected by various types of noise and depend on experimental conditions such as cell line, tissue, gene expression levels, stress conditions etc., paving the way for the *in silico* modeling of RNA-protein interactions.

Results: Here we present ProtScan, a predictive tool based on consensus kernelized SGD regression. ProtScan denoises and generalizes the information contained in CLIP-seq experiments. It outperforms competitor state-of-the-art methods and can be used to model RNA-protein interactions on a transcriptome-wide scale.

Availability: ProtScan is available at https://github.com/gianlucacorrado/ProtScan/

Contact: f.costa@exeter.ac.uk

[*]To whom correspondence should be addressed: `f.costa@exeter.ac.uk`

1 Introduction

RNA-binding proteins (RBPs) are regulating many vital aspects of transcribed RNA such as splicing, maturation, stability and translation. Recent studies (Baltz *et al.*, 2012; Castello *et al.*, 2012; Ray *et al.*, 2013; Gerstberger *et al.*, 2014) estimated that the human genome encodes more than 1500 RBPs. This implies that the complexity of post-transcriptional regulation by RBPs is matching that of the regulation by transcription factors (Vaquerizas *et al.*, 2009). An important step to understand this layer of regulation is to detect binding sites of RBPs on regulated RNAs. In this context, CLIP-seq (cross-linking and immunoprecipitation followed by next generation sequencing) (Licatalosi *et al.*, 2008) together with its modifications PAR-CLIP (Hafner *et al.*, 2010), iCLIP (König *et al.*, 2010), and eCLIP (Van Nostrand *et al.*, 2016) has become the state-of-the-art procedure for determining transcriptome-wide binding sites of RBPs, resulting in libraries of reads that are bound and protected by a specific RBP.

There are two important tasks in the *in silico* analysis of CLIP-seq data for an individual RBP. The first obvious task is the reduction of the false positive rate by removing reads that correspond to unspecific binding. This is the task of peak calling, which determines regions that are enriched in CLIP-seq reads and thus are likely bound by the RBP used in the CLIP-seq experiment. Some popular peak calling tools are PARalyzer (Corcoran *et al.*, 2011), Piranha (Uren *et al.*, 2012) and CLIPper (Lovci *et al.*, 2013).

The second task is less obvious but possibly even more important, namely the reduction of the false negative rate. False negatives are RNAs that are bound by the RBPs but not detected in the CLIP-seq experiment. It turns out that the false negatives are the major obstacle in using publicly available CLIP-seq data to investigate biological questions related to RBPs. The reason is that target sites identified by CLIP-seq depend on the transcriptome state of the cells used for the CLIP-seq experiment, as the associated target transcripts have to be expressed at certain levels to be detected. Thus, using these sites for analyzing biological questions in cells with different transcriptome states is suboptimal and can fail to detect many important sites, leading to wrong biological conclusions. To give an example, Ferrarese *et al.* (2014) investigated the role of the splice factor PTBP1 in differential splicing of the tumor suppressor gene ANXA7 in glioblastoma. Albeit there was strong biological evidence for PTBP1 directly binding ANXA7, no binding site was found in a publicly available CLIP-seq dataset for PTBP1. Instead, only a computational analysis was capable to detect and correctly localize the presence of potential binding sites which were then experimentally validated.

In the last years, several specialized CLIP-seq databases have appeared like doRiNA (Anders *et al.*, 2011) and others ranging from those focused on in- vitro and in-vivo experiments (Cook *et al.*, 2010) to those that offer transcriptome-wide visualizations (Khorshid *et al.*, 2010). In

the literature, approaches to predict RBP binding sites range from the adaptation of tools built for DNA-binding motifs of transcription factors (see (Das and Dai, 2007) for a survey) to specialized approaches that can take the RNA folding properties into account. Well-known motif finder algorithms of the first type include MEME (Bailey *et al.*, 1994), MatrixREDUCE (Foat *et al.*, 2006) and DRIMust (Leibovich *et al.*, 2013). Applications of these tools to the analysis of RBPs are described in (Sanford *et al.*, 2009; Kazan *et al.*, 2010; Gupta *et al.*, 2013). Approaches developed explicitly for RNA motives include MEMERIS (Hiller *et al.*, 2006) (an extension of MEME biased towards single- stranded RNA regions) and RNAContext (Kazan and Morris, 2013) (which distinguishes the type of unpaired regions between e.g. bulges, multiloops and hairpins). mCarts (Zhang *et al.*, 2013) is a tool based instead on a Hidden Markov Model (HMM) that takes into account the number and the distance between targets in addition to evolutionary conservation information (Zhang et al. 2013). More recently Maticzka *et al.* (2014) introduced a graph kernel approach showing improved performance over motif-based techniques.

Here we propose a novel method called ProtScan that uses a combination of kernelized regression with consensus voting in order to localize the protein binding sites. The key idea is to cast the identification of target regions in long RNA sequences as a regression task over short *moving* windows, where the regressed information is the distance to the closest target. It is well known (Hansen and Salamon, 1990; Perrone, 1993; Krogh *et al.*, 1995; Breiman, 2001) that when the classifiers in an ensemble are both individually strong and collectively *diverse*, the consensus prediction is on average better than that of any individual classifier. In our case we want to train different predictors with sequences that are at different distances from the target site. The intuition is that at different distances there will be different clues that could hint at the presence of a nearby target site. Finally, instead of having multiple classifiers, one for each different distance value, we train a single regressor to directly predict the distance value.

After introducing the details of the proposed method in Section 2, in Section 3 we empirically investigated the following questions: Q1) is there an advantage in formulating the problem as a regression task rather than a standard classification task? Q2) is the feature representation obtained by string kernel methods competitive w.r.t. other state-of-the-art approaches (e.g. based on deep artificial neural networks)?

2 Materials and Methods

The ProtScan pipeline is composed of several steps that can be aggregated into two main components: the first one models RNA-protein interactions and is used to predict the interaction profiles, while the second identifies binding sites as significant peaks in these profiles. In the following we give a brief overview of the processing flow (see Figure 1).

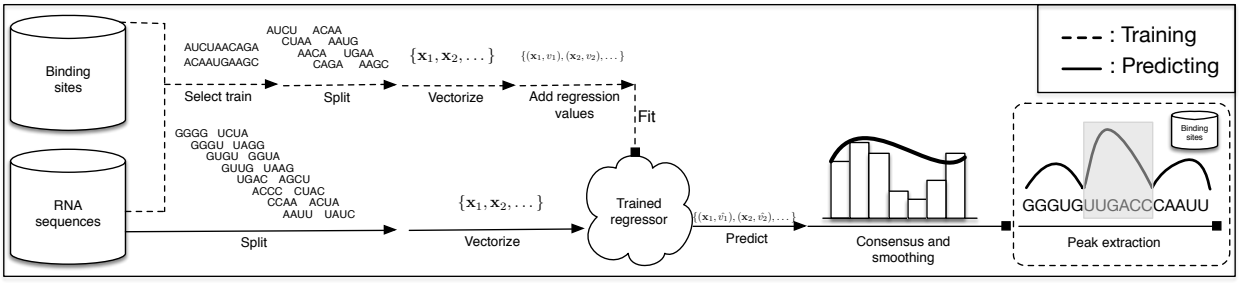

Figure 1: Workflow depicting the steps required for training a ProtScan model (dashed lines) and for predicting interaction profiles using a trained model (solid lines). The dashed box represents the peak extraction step.

The first component estimates RNA-protein interaction profiles using a combination of kernelized regression with consensus voting. The kernelized regression has the task to estimate the distance of a portion of the RNA from the closest binding site, while the consensus voting is used to aggregate the predictions from the different regions. The regressor is trained using experimentally verified binding sites (dashed lines in Figure 1). First, we select an informative set of fixed-length RNA fragments for training. We distinguish positive fragments, when these are centered on a protein binding site, and negative fragments, when these are sampled at random in RNA regions that are far from binding sites. The fragments are further split into smaller overlapping windows, which are transformed into sparse vectors using a kernelized approach. We annotate each window with its distance from the closest binding site, and use a special value for the negative windows. Finally, we learn a regressor to predict the association between windows and their distance to the closest binding site.

In the test phase, we compute the interaction profile for a set of arbitrarily long RNA sequences (solid lines in Figure 1). First, each RNA is split into small overlapping windows. The windows are then mapped to vectors, and their distance from the closest binding site is assessed using the trained regressor. All distances are then aggregated in a histogram for consensus voting. Finally, the counts are smoothed to obtain the RNA-protein interaction profile with single-nucleotide resolution.

The second component extracts the most reliable interactions from the predicted profiles. It can therefore be used to *denoise* a CLIP-seq experiment, removing protocol artifacts and biases. Starting from the predicted profiles generated by the first component, ProtScan identifies all the peaks and then, using the experimental evidence as control, selects peaks above a desired significance level (dashed box in Figure 1).

2.1 Dataset

We use data obtained with the enhanced CLIP (eCLIP) (Van Nostrand *et al.*, 2016) protocol. We downloaded BED narrowPeak files, containing the output of the analysis pipeline of human eCLIP experiments, from the ENCODE project website (Sloan *et al.*, 2016) (April 2016 release). The BED narrowPeak files contain the genomic coordinates of RBP binding regions and their respective *fold change* values, i.e. the base 2 logarithm of the ratio between the number of aligned reads in the CLIP and the ones in the RNAseq control library. Higher fold change values are indicative of more reliable binding regions.

The full dataset includes 96 RBPs, with experiments performed in two different cell lines, i.e. K562 and HepG2 (38 RBPs on both cell lines, 40 only on K562 and 18 only on HepG2). Each experiment, identified by a protein and a cell line, is performed in two replicates. The presence of two replicates allows us to perform quality control on the data and it allows us to select only stable experiments. We define *binding sites* as regions with a fold change higher than a user-defined threshold. By setting the threshold to 2.0 and 3.0 respectively, we identify two increasingly stringent sets of binding sites. This allows us to compare the robustness of predictive methods for different levels of data quality. For each set, we then discard experiments where the total number of binding sites across the two replicates varies by more than 15%. A subset of 46 different RBPs passes this quality control, 8 having experiments on both cell lines, 25 only on K562 and 13 only on HepG2. When looking at the fold change threshold, 20 RBPs pass the quality control at both values, 22 only at 2.0 and 4 only at 3.0.

The BED narrowPeak files report the binding regions in genomic coordinates (hg19 assembly), but for the scope of this work we are interested in working with full-length gene sequences. First, genomic coordinates are converted from hg19 to hg38 assembly using the UCSC's liftOver tool (Speir *et al.*, 2016). Afterwards, genomic coordinates are converted to gene coordinates using the human cDNA GTF file from Ensembl as a reference (release 84) (Yates *et al.*, 2015).

More formally, for each RNA sequence r we define the set $\mathcal{B}^r$ of coordinates b, where $b = (e - s)/2$ is the center of a binding site on r that starts at coordinate s and ends at coordinate e. If an RNA sequence r has no binding sites, then $\mathcal{B}^r = \varnothing$.

2.2 Interaction profile predictor

In the following we detail the steps for the RNA-protein interaction profile estimator (Figure 1).

Selection of training subsequences. Training subsequences are selected in order to include information surrounding experimentally determined binding sites (positive RNA subsequences) as well as "background" information from RNA portions far away from any binding site (negative RNA subsequences). Each positive subsequence is centered on a binding site and

is extended d_{max} nucleotides on both sides for a total length of $2d_{max}$. Negative subsequences have the same length but are centered on nucleotides more than d_{max} nucleotides away from the center of any binding site. Since including a huge number of negatives that overwhelms the number of positives might cause improper training of the regressor, we select at random a number of negative subsequences that is proportional to the number of positive ones (*negative_ratio* times the number of positives). Both d_{max} and *negative_ratio* are hyperparameters of the model that can be optimized with the the random search hyperparameter optimization procedure of ProtScan (see Supplementary material).

Splitting. Each sequence r of length l (when considering training subsequences $l = 2d_{max}$) is split in overlapping windows of size $split_window < l$. Each window is identified by the position i of its central nucleotide on r. The amount of overlap between two consecutive windows is controlled by the parameter *split_step* with $split_step < split_window$ (the strict inequality ensures overlap).

Vectorization. A typical approach to process non-vector data (such as sequences or graphs) is to employ the "kernel trick" (Shawe-Taylor and Cristianini, 2004). The trick consists in using an algorithm that interacts with the input only in terms of inner product between instances. All that is needed then is a way to efficiently define an inner product between discrete sequences. A typical solution is offered by string kernels (Leslie *et al.*, 2002) that compute the fraction of common k-mers (i.e. short subsequences of length k). Here, for efficiency reasons, we use a different approach and compute an explicit feature mapping from discrete sequences x to sparse vectors in very high dimensional spaces $\mathbb{R}^d$, where d is typically in the order of tens of thousands. To do this we follow the Neighborhood Subgraph Pairwise Distance Kernel (NSPDK) approach proposed in (Costa and De Grave, 2010) and define a feature construction procedure $\phi_k(x) \mapsto \mathbb{R}^d$ that returns the histogram of the occurrences of each k-mer in a string x. A hash function $h : \Sigma^* \mapsto \mathbb{N}$ is used to map k-mers (short strings in a finite alphabet Σ) to the corresponding integer codes $n \in \mathbb{N}$ in the addressable space (i.e. $n < d$). In order to take into account the contribution of k-mers of different complexities (different values of k) in a balanced way, we first consider the normalized version: $\hat{\phi}_k(x) = \phi_k(x)/\sqrt{< \phi_k(x)\phi_k(x) >}$, then we combine the vector representations for different orders k in a single vector: $\phi_C(x) = \sum_{k=0}^{C} \hat{\phi}_k(x)$ and finally we output the normalized result: $\hat{\phi}_C(x) = \phi_C(x)/\sqrt{< \phi_C(x)\phi_C(x) >}$. We call the maximum k-mer size C, the *complexity* of the vectorization. When C is small (say below 10), the number of non-zero features per sequence is small (there can be maximally as many distinct features as C times the length of the sequence), yielding an efficient computation for the downstream learning algorithm. Note that the normalization changes the representation from a list of counts to a list of proportions. In practical terms this means that instead of considering the number

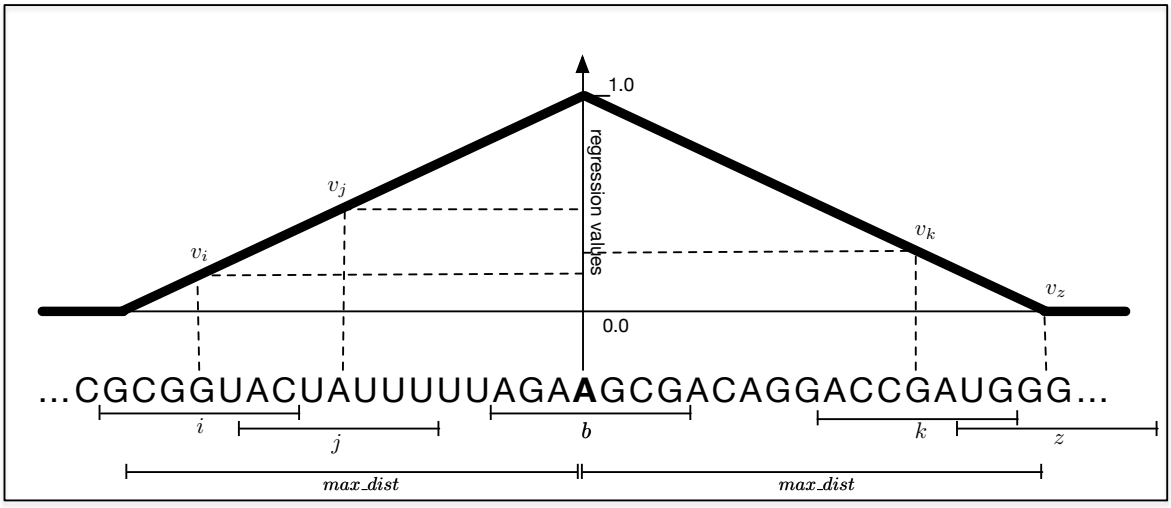

Figure 2: Example of the definition of regression values. The regression value v_i is lower than v_j because window i is farther from the target site b than window j. Although window k is positioned upstream from the binding site b and windows i and j are downstream, $v_i < v_k < v_j$ because the regression values do not need to account for the relative position w.r.t. the binding site but only for the absolute distance. Moreover, $v_z = 0$ because the center of the window z is located at d_{max} nucleotides from the binding site b.

of occurrences of a k-mer in a sequence we consider its frequency. To fix ideas, when $C = 6$ (the value which was found optimal by the cross validation selection procedure on most RBP tasks in our experimental evaluation), NSPDK will generate features for $k \in \{1, 2, 3, 4, 5, 6\}$, i.e. ranging from the nucleotide composition ($k = 1$), to the di-nucleotide composition, up to the 6-mers composition. Note that larger values of k increase the complexity of the method until it starts to memorize idiosyncratic aspects of the training data and the predictive performance on future instances degrades.

Regression. In ProtScan we employ a ridge regressor with squared loss and l_2 regularization trained using stochastic gradient descent (SGD). Let i be the center of a window of a RNA sequence r, then v_i is the corresponding regression value which is inversely proportional to the distance of i from the closest binding site on sequence r, if i is a positive window, and zero otherwise

$$v_i = \begin{cases} \max(0, 1 - \frac{\min_{b \in \mathcal{B}^r} |i-b|}{d_{max}}) & \text{if } \mathcal{B}^r \neq \emptyset \\ 0 & \text{otherwise} \end{cases} \quad (1)$$

In the prediction step, we estimate the distance values for RNA windows of test RNA sequences. For each test window i, the regressor predicts a value $\hat{v}_i$. The predicted value is mapped to a distance $\hat{d}_i \in [0, d_{max}]$ inverting Equation 1:

$$\hat{d}_i = d_{max} * (1 - \hat{v}_i) \tag{2}$$

Note that Equation 1 assigns regression values according to the *absolute* value of the distance from the most adjacent binding site (Figure 2) and that it cannot recover the relative position of the window with respect to the binding site (i.e. downstream or upstream). Encoding directionality information using, for example, negative regression values to indicate upstream locations yielded poor performance due to the discontinuity at zero. As we will show now, the exact location can be recovered using a consensus voting procedure.

Consensus voting and smoothing. In the test phase we aggregate the predictions from all available windows. We build a histogram $\mathbf{h} = (h_1, \ldots, h_l)$, where l is the length of a test RNA sequence r and h_j aggregates the votes received by its j-th nucleotide. We discard a window i if $\hat{v}_i \leq 0$ as it is predicted to be too far from a binding site to be relevant. Otherwise, every prediction contributes two votes, one upstream to position $i - \hat{d}_i$ and one downstream to $i + \hat{d}_i$ (recall that the regressor is trained over the absolute value of the distance). Votes for position j are thus computed as:

$$h_j = \sum_{i \in windows(r)} \begin{cases} \hat{v}_i & \text{if } i \pm \hat{d}_i = j \text{ and } \hat{d}_i < d_{max} \\ 0 & \text{otherwise} \end{cases} \qquad \forall j \tag{3}$$

In Equation 3 each vote is weighted according to the predicted distance, i.e. the closer the voting window the higher the weight. This is done to impose a bias whereby RNA windows that are closer to a binding site are considered more important for the protein recognition than more distant windows. Development experiments (not reported) indicate that vote weighting has a marginal but beneficial effect on the predictive performance estimate. Secondly, the vote is added to both $i \pm \hat{d}_i$, i.e. upstream and downstream from the window coordinate. At first glance, this seems an issue, as one of the two votes is clearly wrong. However, votes will combine in a constructive way only on the true location while they will incoherently spread out in the other direction (see Figure 3).

Finally, Gaussian smoothing, i.e. the convolution of histogram $\mathbf{h}$ with a Gaussian $\mathcal{N}(\mu, \sigma)$, is applied to the histogram $\mathbf{h}$ to denoise it and to produce a single-nucleotide resolution interpolated profile.

Hyperparameter selection. ProtScan exhibits a relatively large set of hyperparameters (see Supplementary Material), which we optimize using a two-fold cross validation random search approach (Bergstra and Bengio, 2012). By running the hyperparameter optimization over 34 models for 11 different RBPs for the comparison with the related work (Section 3.1),

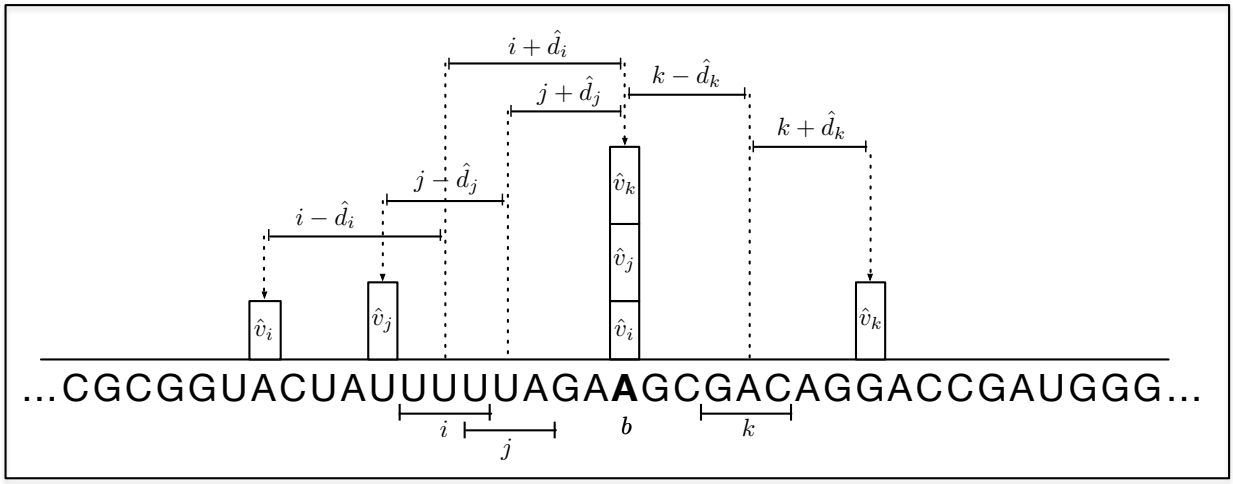

Figure 3: Example of the consensus voting approach. Under the assumption that the regressor is perfectly trained ($\hat{v}_c = v_c$ for all windows c), $\hat{d}_c$ represents the exact distance of a window c to the closest binding site b. From the example it is possible to notice that the votes are correctly piling up on the binding site and spreading on the other nucleotides.

we noted that several optimal hyperparameter values where stable for a wide range of RBPs (see Supplementary Material for details). These results are now incorporated as default parameters and allow to train ProtScan on novel RBPs, skipping the computationally expensive hyperparameters optimization phase while maintaining high predictive performance.

2.3 Peak extraction

Predicted interaction profiles consist of single-nucleotide resolution signals indicative of the RNA-protein coupling. However, the localization of significant peaks in these profiles is a non-trivial task, akin the process of peak calling in CLIP-seq data analysis. We therefore implemented a similar approach to find significant peaks and thus sites likely bound by the RBP from the predicted interaction profiles.

To do so we first extract all the peaks in the predicted profiles using a variant of the *mean shift* algorithm (Comaniciu and Meer, 2002). Mean shift scans a sequence with a fixed-length sliding window and records the maximum value found in each window. It then iteratively repeats the procedure over the sequence of maxima found until no further change occurs. An analogous procedure is used to localize all the minima. After identifying all the local maxima and minima in the profile, we define a candidate predicted binding site as a *block* $b = (s, e)$ with coordinates $(s, e) : s < e$. If both s and e are minima, the block contains no other minimum and at least one maximum.

In order to select the subset of significant binding sites among the extracted peaks, we compare them with a background distribution fit on negative data. First, a cumulative Gaussian

distribution for the maximum is fit over the height of the blocks coming from transcripts without experimental evidence of binding (negative examples). Second, each candidate block is accepted as significant if it stays in the top θ^{th} percentile of the distribution, with θ specified by the user. The procedure is cross validated two-fold to avoid overfitting.

3 Results and discussion

Amongst popular methods to model target regions for RBPs there are approaches based on Position Specific Score Matrices (PSSM), such as MEME (Bailey *et al.*, 1994) or DREME (Bailey, 2011). In the following we exploited the results reported in Maticzka *et al.* (2014) that show how more sophisticated approaches that can model higher order correlations between nucleotides exhibit greater predictive performance and hence compare directly against GraphProt (Maticzka *et al.*, 2014).

Unfortunately the comparison to other kernel approaches (such as the spectrum kernel of Leslie *et al.* (2002)) is hindered by computational complexity issues. Kernel methods that do not produce an explicit feature encoding, in fact, cannot be easily applied to transcriptomic or genomic scale data since their complexity grows quadratically with the number of fragments or regions considered. For this reason we resorted to compare ProtScan with a state-of-the-art method based on a deep neural network architecture called DeepBind (Alipanahi *et al.*, 2015).

3.1 Comparison with related work

GraphProt (Maticzka *et al.*, 2014) is an SVM-based classifier with a graph kernel developed for RNA molecules, trained to predict sequence- and structure-binding preferences of RNA-binding proteins from high-throughput experimental data. DeepBind (Alipanahi *et al.*, 2015) uses deep convolutional neural networks (CNNs) to model RNA-protein binding patterns from RNAcompete data (Ray *et al.*, 2009).

The comparison was performed on a subset of 11 RBPs from our dataset (Section 2.1) for which a pre-trained DeepBind model is available (training a DeepBind model is computationally very expensive and requires powerful hardware like a GPU cluster). For each protein, multiple tests were performed considering different cell lines, fold change values to define binding sites from experimental evidence, and technical replicates, for a total of 34 comparisons. In this comparison, we tested the performance of the three approaches on $\sim 1\%$ of human genome ($\sim$ 600 protein coding and non-coding genes). The test genes were selected at random, keeping the same ratio between bound and unbound genes that is present in the full dataset.

We computed the interaction profiles for ProtScan as explained in Section 2.2. GraphProt and DeepBind were originally designed for a binary classification task, i.e. to identify whether

Table 1: Performance comparison among GraphProt (Maticzka *et al.*, 2014), DeepBind (Alipanahi *et al.*, 2015) and our method, ProtScan, on 11 RBPs. For each test protein, multiple tests were performed taking into consideration different cell lines (CL), fold changes (FC), and replicates (R), for a total of 34 comparisons. For each comparison, the best score is highlighted in boldface.

				AUC ROC		
RBP	**CL**	**FC**	**R**	**GraphProt**	**DeepBind**	**ProtScan**
FMR1	K562	2.0	1	0.83	0.63	**0.88**
			2	0.80	0.62	**0.84**
GTF2F1	HepG2	2.0	1	0.71	0.56	**0.80**
			2	0.78	0.58	**0.86**
		3.0	1	0.72	0.56	**0.79**
			2	0.80	0.58	**0.86**
HNRNPA1	HepG2	2.0	1	0.72	0.76	**0.81**
			2	0.72	0.75	**0.82**
	K562	2.0	1	0.72	0.77	**0.80**
			2	0.72	0.74	**0.83**
		3.0	1	0.71	**0.77**	**0.77**
			2	0.72	0.74	**0.80**
HNRNPC	HepG2	2.0	1	0.68	**0.86**	**0.86**
			2	0.71	0.77	**0.87**
HNRNPK	K562	3.0	1	0.81	0.86	**0.89**
			2	0.79	0.85	**0.90**
IGF2BP2	K562	2.0	1	0.75	0.29	**0.80**
			2	0.76	0.31	**0.79**
IGF2BP3	HepG2	2.0	1	0.66	0.35	**0.85**
			2	0.70	0.35	**0.82**
KHDRBS1	K562	2.0	1	0.60	0.64	**0.64**
			2	0.62	0.63	**0.66**
QKI	HepG2	2.0	1	0.59	0.68	**0.74**
			2	0.54	0.56	**0.74**
		3.0	1	0.58	0.68	**0.72**
			2	0.54	0.56	**0.69**
TARDBP	K562	2.0	1	0.71	0.84	**0.88**
			2	0.72	0.86	**0.88**
U2AF2	HepG2	2.0	1	0.59	0.68	**0.76**
			2	0.59	0.68	**0.72**
	K562	2.0	1	0.59	0.69	**0.78**
			2	0.62	0.67	**0.79**
		3.0	1	0.59	0.69	**0.76**
			2	0.62	0.67	**0.77**
			AVG	**0.69**	**0.65**	**0.80**
			STD	**0.08**	**0.15**	**0.07**

a RNA sequence contains a RBP binding site, but they were not designed to model interactions at single-nucleotide resolution. Despite that, GraphProt allows to partition the feature set according to each nucleotide. This enables the marginalization of the weights induced by the linear estimator and extract a nucleotide-wise interaction profile. We adapted DeepBind using an approach similar to the one used in ProtScan, i.e. we split the RNA in overlapping windows and we aggregated the score of all the windows (see the Supplementary Material for details).

Note that modeling binding sites at single-nucleotide resolution is a much harder task than the binary interaction classification prediction. First, the amount of predictions is significantly higher: from one per RNA sequence to one per nucleotide. Second, and more importantly, when considering long RNA sequences, the ratio between interacting and non-interacting nucleotides is extremely small, resulting in a drastically unbalanced prediction task (the average ratio in our dataset is 1 to 2500).

Table 1 reports the AUC ROC results for each RBP, computed over all target transcripts and positions. AUC ROC measures the quality of the ranking, allowing to compare interaction profiles on different scales. In fact, a perfect AUC ROC score of 1.0 is achievable only when all the interacting nucleotides of the test sequences obtained higher interaction scores than the non-interacting ones. It is important to note that the AUC ROC values reported in Maticzka *et al.* (2014) and Alipanahi *et al.* (2015) are on a different task, namely on a balanced binary classification. The experiments show that ProtScan outperforms the other approaches nearly always (except for two cases in which it ties with DeepBind). With an average AUC ROC of 0.8, ProtScan achieves a relative AUC ROC improvement of 35% over GraphProt, and of 43% over DeepBind. Performing a paired analysis, we observed that ProtScan outperforms GraphProt in all 34 cases, and DeepBind in 32 out of 34 ones (with two ties). The paired analysis between GraphProt and DeepBind revealed that the former has a better average AUC ROC while the latter wins in terms of pairwise comparisons (24 wins out of 34 cases). We note that the average AUC ROC of DeepBind was severely penalized by the scores obtained for two proteins (IGF2BP2 and IGF2BP3). It has been speculated that the IGF2BP family proteins (IGF2BP1-3) possess more complex binding patterns due to the presence of multiple RNA- binding domains (Hafner *et al.*, 2010). In fact it was shown for IGF2BP1 that the RBP relies on two RNA-binding sites, which can be found at varying distances and orientations in functional target sequences (Patel *et al.*, 2012). However, since DeepBind models were trained on RNAcompete data, they rely on local sequence motifs, which could be insufficient to represent two or more disconnected binding sites. The good predictive score of ProtScan indicates that the use of a much larger sequence context can help to identify these complex binding patterns also in the case of IGF2BP family proteins.

In the supplementary material we also report the area under the precision recall curve

(auPRC), which is a performance measure suitable for highly unbalanced predictive tasks. The results indicate, consistently, that ProtScan outperforms DeepBind (wins/ties/loses 20/11/3), that GraphProt and DeepBind are compatible (W/T/L 11/9/14) and that ProtScan markedly improves on GraphProt (27/7/0). The average (median) auPRC for the methods was 0.008 (0.006) (ProtScan), 0.003 (0.001) (DeepBind) and 0.002 (0.001) (GraphProt).

Discussion. We can now address the two questions: Q1) is there an advantage in formulating the problem as a regression task rather than a standard classification task? Q2) is the feature representation obtained by string kernel methods competitive w.r.t. other state-of-the-art approaches (e.g. based on deep artificial neural networks)?

A1) The comparison between ProtScan and GraphProt hints at a positive answer. The two approaches are based on the same technique to map sequences to a vector space and differ only in the way the task is formulated. We conjecture that the regression formulation together with the consensus voting and the subsequent smoothing yields a predictor with a smaller variance and hence a smaller predictive error. By averaging multiple predictions, we have effectively created an ensemble classifier where the diversity between predictors is enforced by training each predictor with sequences at different distances from the target. Using a single predictor in a regression task, rather than multiple predictors for each possible distance value, is a way to tie together the various predictions and can be seen as a form of additional regularization.

A2) Unfortunately we do not have a clear answer to this question. First of all, the predictive performance of GraphProt and DeepBind (both trained using only local information around the target regions) is comparable so there is no clear winner. Secondly, the datasets used in their respective training phases stem from different experimental methods. While GraphProt models were trained on *in vivo* RBP binding sites determined by eCLIP, DeepBind models were trained on RNAcompete data, which consist of short *in vitro* RBP-bound sequences. The effect of a different training regime is therefore a confounder in trying to assess whether a direct k-mer based representation is sufficient or indeed preferable to the distributed representation employed by neural network architectures. However, it can stated that the discrete representation is not markedly worse and is computationally much faster to train.

3.2 Transcriptome-wide target site modeling

ProtScan can be used to model RNA-protein interactions and to predict interaction profiles at a transcriptome-wide scale. As examples we considered the two vastly studied RBPs HNRNPA1 and FMR1. These RBPs act in different cellular compartments, i.e. the nucleus for HNRNPA1 and the cytoplasm for FMR1. Nuclear RBPs, especially splice factors such as HNRNPA1, interact with pre-(m)RNA that is composed of introns and exons, while cytoplasmic RBPs

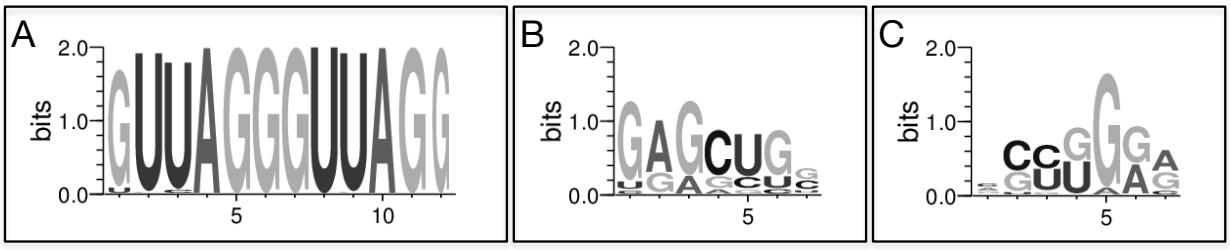

Figure 4: Motifs obtained analyzing the top 5,000 peaks extracted from the transcriptome-wide predicted profiles generated by ProtScan. (A) The 12-mer GUUAGGGUUAGG resembles the consensus high affinity HNRNPA1 binding site UAGGG(A|U) identified in Burd and Dreyfuss (1994). (B-C) The 7-mer GAGCUGG and all the 6-mers matching the following regular expression (C|G)(C|U)(G|U)G(G|A)(A|G) resemble the consensus motifs ACUG and UGGA obtained in Ascano *et al.* (2012) analyzing high-throughput data of the FMR1 protein.

such as FMR1 interact with mature RNA molecules, from which the intronic sequences have been removed during splicing. Note that dealing with mature RNAs and ignoring intronic sequences shortens the computation time required for predicting the binding profiles of an order of magnitude.

HNRNPA1: HNRNPA1 is member of a family of ubiquitously expressed heterogeneous nuclear ribonucleoproteins (hnRNPs) which associate with pre-(m)RNAs in the nucleus and influence their processing, as well as other aspects of RNA metabolism and transport. HNRNPA1 is one of the most abundant core proteins of hnRNP complexes and plays a key role in the regulation of alternative splicing. Mutations in the HNRNPA1 gene have been observed in individuals with amyotrophic lateral sclerosis (ALS) (Geuens *et al.*, 2016). We considered the eCLIP experiment on K562 cells (replicate 1) and select HNRNPA1 binding sites with a fold change threshold of 2.0, resulting in 4,964 interaction sites. We generated interaction profiles for the entire set of human genes using a two-fold cross-prediction procedure analogous to the one employed for peak extraction (using in turn one subset for training and the other for prediction), obtaining an overall AUC ROC of 0.85.

Next, we extracted the significant peaks from the predicted interaction profiles as proposed to Section 2.3 and visualized the target regions identified by ProtScan by running a motif finder procedure on the 5,000 peaks with the lowest p-value. An *in vitro* study by Burd and Dreyfuss (1994) identified the motif UAGGG(A|U) as a consensus high affinity HNRNPA1 binding site. This consensus sequence is well represented in the HNRNPA1 motif displayed in Figure 4A. The 12-mer GUUAGGGUUAGG occurs 63 times (exact match) in the analyzed subsequences.

FMR1: In contrast to HNRNPA1, FMR1 is known to associate with polysomes, and an expansion of the CGG repeat in the 5' UTR of the FMR1 gene is known to cause the fragile X syndrome (FXS) (Richter *et al.*, 2015). We considered the eCLIP experiment on K562 cells

(replicate 1) and selected FMR1 binding sites with a fold change threshold of 2.0, obtaining 26,732 interaction sites. The fact that FMR1 is usually located at polysomes in the cytoplasm allows us to consider only mature RNAs, i.e. RNAs without intronic sequences. In humans, alternative splicing enables the production of more than one transcript from each gene. In order to not consider every splice variant of each gene, we selected the most prominent transcript through a series of hierarchical filtering steps: first we considered the transcript support level (TSL) that identifies well supported transcripts, then the APPRIS annotation (Rodriguez *et al.*, 2012) that annotates principal splicing isoforms, followed by the GENCODE basic annotation that identifies the representative transcripts of a gene, and finally the transcript length (preferring longer transcripts). If the procedure ended up producing two or more transcripts (which are on par on all parameters), the most prominent transcript was selected at random among them. The selection of the most prominent transcript for each gene allowed to significantly reduce the size of the dataset and, therefore, to speed up the prediction of the interaction profiles for this RBP. Cross-predicted interaction profiles achieved an AUC ROC of 0.79.

As with HNRNPA1, we visualized the FMR1 target regions obtained from the analysis of the 5,000 peaks at lowest p-value. A PAR-CLIP study of FMR1 target sites (Ascano *et al.*, 2012) identified two distinct motifs for this RBP: ACUG and UGGA. These motifs are in substantial agreement with those extracted from the ProtScan profiles. The 7-mer GAGCUGG (Figure 4B) occured 445 times (exact match) in the considered subsequences, while the 6-mers matching the following regular expression (C|G)(C|U)(G|U)G(G|A)(A|G) (Figure 4C) were found 4233 times.

The sufficiently high AUC ROC scores indicate that ProtScan can be used to reliably model the interaction profiles on a transcriptome-wide scale. The agreement between the resulting motifs and those identified in *ad hoc* studies (Burd and Dreyfuss, 1994; Ascano *et al.*, 2012) additionally supports the quality of the predicted interaction profiles.

3.3 Validated predictions

We show that ProtScan can identify valid candidate locations even in the absence of a significant signal in the CLIP data for a given region of interest. Here we used the 6 PTBP1 binding sites predicted by GraphProt on the ANXA7 gene and subsequently verified by mutation experiments (Ferrarese *et al.* (2014)) (see Supplementary Table 3). We trained both a GraphProt and a ProtScan model on the available PTBP1 K562 eCLIP binding sites. For model training, 2718 positive sites were used for GraphProt (fold change ¿ 4.2) and 11630 for ProtScan (fold change ¿ 3). Note however that the PTBP1 eCLIP quality does not satisfy the requirements used in the previous experiments, since the binding site are not sufficiently consistent across replicates. Notwithstanding the lower quality, ProtScan can learn a reliable predictive model. In more details, nucleotide wise binding scores on the full ANXA7 gene sequence (taken from Ensembl

human genes GRCh38.p10) were predicted for both methods. Nucleotide wise predictions were additionally calculated on a set of 5000 randomly selected transcript sequences (same Ensembl release) in order to generate an empirical distribution for the background model. To extract top-scoring regions, we only considered contiguous regions with p-value ¡ 0.05 and checked the overlap with the experimentally verified PTBP1 binding sites. For GraphProt, 9 of a set of 368 regions deemed significant overlapped with 6 of 6 verified PTBP1 binding sites, while for ProtScan 3 of 34 proposed regions were overlapping with 3 of 6 verified PTBP1 binding sites. These results indicate that while GraphProt's recall is higher it also tends to predict a larger number of locations than ProtScan and is therefore likely to exhibit a lower precision. Equating the non verified proposals sites to false positives we can compute a balanced F-measure (i.e. the harmonic mean of precision and recall) of 0.05 for GraphProt and three times larger (0.15) for ProtScan.

4 Conclusion

In this work we presented ProtScan, a tool based on kernelized regression and consensus voting for modeling and predicting RNA-protein interaction profiles. Extensive experimental results show that the tool is competitive w.r.t. two state-of-the-art approaches (Maticzka *et al.*, 2014; Alipanahi *et al.*, 2015), and that it can reliably be used in a transcriptome-wide setting. In addition to the software, we release 146 ProtScan models for 46 RBPs, induced from eCLIP experiments performed in different cell lines (HepG2 and K562), in dual replicates, and considering different fold change thresholds for selecting the binding sites for training (see Section 2.1).

To further improve the performance of ProtScan, future implementations could include additional types of information, which are known to be associated with RBP binding, including mRNA accessibility and the presence of target sites for regulatory entities such as miRNAs and other known competitive or cooperative RBPs.

Funding

M.U. and R.B. are funded by the Baden-Wuerttemberg-Stiftung (BWST_NCRNA_008) and the German Research Foundation (DFG grant BA2168/11-1 SPP 1738).

References

Alipanahi, B. *et al.* (2015). Predicting the sequence specificities of DNA-and RNA-binding proteins by deep learning. *Nature biotechnology*, **33**(8), 831–838.

Anders, G., Mackowiak, S. D., Jens, M., Maaskola, J., Kuntzagk, A., Rajewsky, N., Landthaler, M., and Dieterich, C.

(2011). dorina: a database of rna interactions in post-transcriptional regulation. *Nucleic acids research*, **40**(D1), D180–D186.

Ascano, M. *et al.* (2012). FMRP targets distinct mRNA sequence elements to regulate protein expression. *Nature*, **492**(7429), 382–386.

Bailey, T. L. (2011). Dreme: motif discovery in transcription factor chip-seq data. *Bioinformatics*, **27**(12), 1653–1659.

Bailey, T. L., Elkan, C., *et al.* (1994). Fitting a mixture model by expectation maximization to discover motifs in bipolymers.

Baltz, A. G. *et al.* (2012). The mRNA-bound proteome and its global occupancy profile on protein-coding transcripts. *Molecular cell*, **46**(5), 674–690.

Bergstra, J. and Bengio, Y. (2012). Random search for hyper-parameter optimization. *Journal of Machine Learning Research*, **13**(Feb), 281–305.

Breiman, L. (2001). Random forests. *Machine learning*, **45**(1), 5–32.

Burd, C. G. and Dreyfuss, G. (1994). RNA binding specificity of hnRNP A1: significance of hnRNP A1 high-affinity binding sites in pre-mRNA splicing. *The EMBO journal*, **13**(5), 1197.

Castello, A. *et al.* (2012). Insights into RNA biology from an atlas of mammalian mRNA-binding proteins. *Cell*, **149**(6), 1393–1406.

Comaniciu, D. and Meer, P. (2002). Mean shift: A robust approach toward feature space analysis. *IEEE Transactions on pattern analysis and machine intelligence*, **24**(5), 603–619.

Cook, K. B., Kazan, H., Zuberi, K., Morris, Q., and Hughes, T. R. (2010). Rbpdb: a database of rna-binding specificities. *Nucleic acids research*, **39**(suppl_1), D301–D308.

Corcoran, D. L. *et al.* (2011). PARalyzer: definition of RNA binding sites from PAR-CLIP short-read sequence data. *Genome biology*, **12**(8), R79.

Costa, F. and De Grave, K. (2010). Fast neighborhood subgraph pairwise distance kernel. In *Proceedings of the 26th International Conference on Machine Learning*, pages 255–262. Omnipress.

Das, M. K. and Dai, H.-K. (2007). A survey of dna motif finding algorithms. *BMC bioinformatics*, **8**(7), S21.

Ferrarese, R. *et al.* (2014). Lineage-specific splicing of a brain-enriched alternative exon promotes glioblastoma progression. *The Journal of clinical investigation*, **124**(7), 2861–2876.

Foat, B. C., Morozov, A. V., and Bussemaker, H. J. (2006). Statistical mechanical modeling of genome-wide transcription factor occupancy data by matrixreduce. *Bioinformatics*, **22**(14), e141–e149.

Gerstberger, S. *et al.* (2014). A census of human RNA-binding proteins. *Nature Reviews Genetics*, **15**(12), 829–845.

Geuens, T. *et al.* (2016). The hnRNP family: insights into their role in health and disease. *Human genetics*, pages 1–17.

Gupta, S. K., Kosti, I., Plaut, G., Pivko, A., Tkacz, I. D., Cohen-Chalamish, S., Biswas, D. K., Wachtel, C., Waldman Ben-Asher, H., Carmi, S., *et al.* (2013). The hnrnp f/h homologue of trypanosoma brucei is differentially expressed in the two life cycle stages of the parasite and regulates splicing and mrna stability. *Nucleic acids research*, **41**(13), 6577–6594.

Hafner, M. *et al.* (2010). Transcriptome-wide identification of RNA-binding protein and microRNA target sites by PAR-CLIP. *Cell*, **141**(1), 129–141.

Hansen, L. K. and Salamon, P. (1990). Neural network ensembles. *IEEE transactions on pattern analysis and machine intelligence*, **12**(10), 993–1001.

Hiller, M., Pudimat, R., Busch, A., and Backofen, R. (2006). Using rna secondary structures to guide sequence motif finding towards single-stranded regions. *Nucleic acids research*, **34**(17), e117–e117.

Kazan, H. and Morris, Q. (2013). Rbpmotif: a web server for the discovery of sequence and structure preferences of rna-binding proteins. *Nucleic acids research*, **41**(W1), W180–W186.

Kazan, H., Ray, D., Chan, E. T., Hughes, T. R., and Morris, Q. (2010). Rnacontext: a new method for learning the sequence and structure binding preferences of rna-binding proteins. *PLoS computational biology*, **6**(7), e1000832.

Khorshid, M., Rodak, C., and Zavolan, M. (2010). Clipz: a database and analysis environment for experimentally determined binding sites of rna-binding proteins. *Nucleic acids research*, **39**(suppl_1), D245–D252.

König, J. *et al.* (2010). iCLIP reveals the function of hnRNP particles in splicing at individual nucleotide resolution. *Nature structural & molecular biology*, **17**(7), 909–915.

Krogh, A. *et al.* (1995). Neural network ensembles, cross validation, and active learning. *Advances in neural information processing systems*, **7**, 231–238.

Leibovich, L., Paz, I., Yakhini, Z., and Mandel-Gutfreund, Y. (2013). Drimust: a web server for discovering rank imbalanced motifs using suffix trees. *Nucleic acids research*, **41**(W1), W174–W179.

Leslie, C. S. *et al.* (2002). The spectrum kernel: A string kernel for SVM protein classification. In *Pacific symposium on biocomputing*, volume 7, pages 566–575.

Licatalosi, D. D. *et al.* (2008). HITS-CLIP yields genome-wide insights into brain alternative RNA processing. *Nature*, **456**(7221), 464–469.

Lovci, M. T. *et al.* (2013). Rbfox proteins regulate alternative mRNA splicing through evolutionarily conserved RNA bridges. *Nature structural & molecular biology*, **20**(12), 1434–1442.

Maticzka, D. *et al.* (2014). GraphProt: modeling binding preferences of RNA-binding proteins. *Genome biology*, **15**(1), R17.

Patel, V. L. *et al.* (2012). Spatial arrangement of an RNA zipcode identifies mRNAs under post-transcriptional control. *Genes & Development*, **26**(1), 43–53.

Perrone, M. P. (1993). *Improving regression estimation: Averaging methods for variance reduction with extensions to general convex measure optimization*. Ph.D. thesis, Brown University.

Ray, D. *et al.* (2009). Rapid and systematic analysis of the RNA recognition specificities of RNA-binding proteins. *Nature biotechnology*, **27**(7), 667–670.

Ray, D. *et al.* (2013). A compendium of RNA-binding motifs for decoding gene regulation. *Nature*, **499**(7457), 172–177.

Richter, J. D. *et al.* (2015). Dysregulation and restoration of translational homeostasis in fragile X syndrome. *Nature Reviews Neuroscience*.

Rodriguez, J. M. *et al.* (2012). APPRIS: annotation of principal and alternative splice isoforms. *Nucleic acids research*, page gks1058.

Sanford, J. R., Wang, X., Mort, M., VanDuyn, N., Cooper, D. N., Mooney, S. D., Edenberg, H. J., and Liu, Y. (2009). Splicing factor sfrs1 recognizes a functionally diverse landscape of rna transcripts. *Genome research*, **19**(3), 381–394.

Shawe-Taylor, J. and Cristianini, N. (2004). *Kernel methods for pattern analysis*. Cambridge university press.

Sloan, C. A. *et al.* (2016). ENCODE data at the ENCODE portal. *Nucleic acids research*, **44**(D1), D726–D732.

Speir, M. L. *et al.* (2016). The UCSC genome browser database: 2016 update. *Nucleic acids research*, **44**(D1), D717–D725.

Uren, P. J. *et al.* (2012). Site identification in high-throughput RNA–protein interaction data. *Bioinformatics*, **28**(23), 3013–3020.

Van Nostrand, E. L. *et al.* (2016). Robust transcriptome-wide discovery of RNA-binding protein binding sites with enhanced CLIP (eCLIP). *Nature methods*, **13**(6), 508–514.

Vaquerizas, J. M. *et al.* (2009). A census of human transcription factors: function, expression and evolution. *Nature Reviews Genetics*, **10**(4), 252–263.

Yates, A. *et al.* (2015). Ensembl 2016. *Nucleic acids research*, page gkv1157.

Zhang, C., Lee, K.-Y., Swanson, M. S., and Darnell, R. B. (2013). Prediction of clustered rna-binding protein motif sites in the mammalian genome. *Nucleic acids research*, **41**(14), 6793–6807.